ORIGINAL RESEARCH

Enhancing Antitumor Efficacy of Nucleoside Analog 5-Fluorodeoxyuridine on HER2-Overexpressing Breast Cancer by Affibody-Engineered DNA Nanoparticle

Chao Zhang[1]
Mengnan Han [ID][1]
Fanghua Zhang[1]
Xueli Yang[1]
Jie Du[1]
Honglei Zhang[1]
Wei Li[1]
Shengxi Chen[2]

[1]College of Chemistry and Environmental Science, Key Laboratory of Chemical Biology of Hebei Province, Laboratory of Medicinal Chemistry and Molecular Diagnosis of the Ministry of Education, Hebei University, Baoding 071002, People's Republic of China; [2]Biodesign Center for BioEnergetics, Arizona State University, Tempe, AZ 85287, USA

Background: Chemotherapy, as an adjuvant treatment strategy for HER2-positive breast cancer, can effectively improve clinical symptoms and overcome the drug resistance of therapeutic monoclonal antibodies. Nucleoside analogues are a class of traditional chemotherapeutic drugs that are widely applied in adjuvant therapy. However, there are many critical issues that limit their clinical efficiency, including poor selectivity and stability, severe side effects and suboptimal therapeutic efficacy. Hence, this work aims to develop a new DNA nanocarrier for targeted drug delivery to solve the above problems.
Methods: Four 41-mer DNA strands were synthesized and 10 FUdR molecules were attached to 5′ end of each DNA strand by DNA solid-phase synthesis. An affibody molecule was connected to the end of polymeric FUdR through a linker in one of the four strands. The affibody-FUdR-tetrahedral DNA nanostructures (affi-F/TDNs) were self-assembled through four DNA strands, in which one vertex was connected to an affibody at the end of a polymeric FUdR tail and three vertices were only polymeric FUdR tails. In vitro cellular uptake of affi-F/TDNs was examined visually with confocal fluorescence microscopy and flow cytometry, and the cytotoxicity of affi-F/TDNs against cancer cells was investigated with MTT assay. Cell apoptosis was detected by Annexin V-FITC/PI double staining method. Using NOD/SCID (Mus Musculus) mice model, the targeted killing efficacy of affi-F/TDNs was also evaluated.
Results: The drug-loading of FUdR in affi-TDNs was 19.6% in mole ratio. The in vitro results showed that affi-F/TDNs had high selectivity and inhibition (81.2%) for breast cancer BT474 cells overexpressing HER2 and low toxicity in MCF-7 cells with low HER2 expression. During the in vivo application, affi-F/TDNs displayed good stability in the blood circulation, achieved specific accumulation in tumor region and the best antitumor efficacy (inhibition ratio of 58.1%), and showed excellent biocompatibility.
Conclusions: The affibody-DNA tetrahedrons, as a simple and effective active targeting delivery nanocarrier, provided a new avenue for the transport of nucleoside antitumor drugs.
Keywords: 5-fluorodeoxyuridine, targeting therapy, her2, breast cancer, affibody, DNA nanoparticle

Correspondence: Honglei Zhang; Wei Li
College of Chemistry and Environmental Science, Key Laboratory of Chemical Biology of Hebei Province, Laboratory of Medicinal Chemistry and Molecular Diagnosis of the Ministry of Education, Hebei University, Baoding 071002, People's Republic of China
Tel/Fax +86 312 592 9009
Email zhanghonglei@hbu.edu.cn; liweihebeilab@163.com

Introduction

Breast cancer is a global disease with the highest incidence among women worldwide, and according to the 2018 Global Cancer Statistics data, new breast cancers globally account for 24.2% of all new malignant tumors, and the mortality rate of breast cancer accounts for 15%.[1] Amplification of HER2 gene occurs in 25–30% of breast cancers

and results in high levels of HER2 protein expression.[2] Thus, the higher expression of HER2 in cancer cells than normal cells and the accessibility of its extracellular domain make HER2 an attractive target for developing targeted therapeutic strategies. Many studies have proved that the antibody therapies against HER2 (Trastuzumab, Pertuzumab, and Ertumaxomab) can significantly improve the therapeutic effect and overall survival rate.[3] However, due to their large molecular weight and humanized construction, monoclonal antibodies have limitations in clinical application, including limited ability to penetrate cells and tissues, the possibility of causing an immune response, and the high cost. Moreover, 40–60% of patients do not respond to the treatment or develop primary and secondary drug resistance to antibody therapy.[4,5] To overcome these limitations, small peptide mimics of antibodies have become attractive alternatives because they are smaller in size and can be easily engineered and modified for specific biological activities.[6] Affibody molecules are the small engineered protein with 58-amino acid residues and three α-helix bundle domains, which can bind a range of different proteins, such as insulin, TNF-a, EGFR, and HER2.[7] Unlike antibodies, HER2-binding affibody molecules have the advantages of much smaller size (~7.0 vs ~150.0 kDa), faster tumor-targeting ability, more well-defined structure, and easier site-specific modification.

In addition, chemotherapy is often used clinically as an adjuvant therapy for antibody therapy to overcome antibody resistance.[8–11] The typical antitumor nucleoside analog, 5-fluorouracil (5-FU), as a component of adjuvant chemotherapy of trastuzumab has been widely applied and achieved satisfactory therapeutic effects against HER2 overexpressing breast cancer.[12–14] It produces activity by incorporating DNA or RNA to inhibit cellular division, and by covalently binding to thymidylate synthase (TS) to inhibit the synthesis of deoxythymidine monophosphate (dTMP) and cause cell death (Figure S1).[15] Although 5-FU has been proved to be a successful therapeutic agent, there still exist a lot of problems in clinical application, such as short half-life (approximately 8–20 mins), poor selectivity, and severe side effects. To circumvent these drawbacks of 5-FU, a variety of organic and inorganic drug delivery systems with nanomaterials have been tested as the alternative approaches to systemic drug administration, such as hydrogels, liposome, Metal-Organic Frameworks (MOFs), boron nitride nanotubes and so on.[16–19] However, considering potential toxicity, lack of tissue specificity, and unsatisfactory clinical results, there are still many defects to be solved.

DNA nanoparticles as drug carriers have the advantages of convenient synthetic process, excellent mechanical rigidity, and structural stability.[20] Meanwhile, DNA also possesses excellent biocompatibility, biodegradability, and low cytotoxicity. Recently, based on the structural similarity to thymidine (T), Mou[21] and Jorge[22] incorporated 5-fluorodeoxyuridine (FUdR, metabolite of 5-FU) into DNA polyhedra and DNA origami, respectively, by covalent ligation using DNA solid-phase synthesis technology, which exhibited an enhanced cytotoxicity related to conventional 5-FU and FUdR. However, the processes of constructing DNA polyhedra and DNA origami are tedious and complicated, and the drug-loading rate is low. In addition, the lack of active targeting also prevents the nanodrug from being adequately taken up by cell, and reduces their antitumor efficacy.

In our previous studies, an antibody-like DNA-affibody nanoparticle was constructed using affibody molecule as a targeting ligand and DNA tetrahedron as a scaffold. Then, this nanoparticle was employed for transporting doxorubicin and cisplatin to specific cancer cells through non-covalent bonding, respectively, to enhance the targeting of drug treatment.[23,24] However, their main issues are the difficulty in accurately controlling drug loading and the leak of chemotherapy drugs during in vivo transport.[25] These are the main obstructions in the development and clinical application of this kind of nanodrugs. Thus, in this study, a new affibody-DNA tetrahedron nanoparticle loaded with FUdRs by covalent bonds was prepared. The nano-structural drug contained one DNA tetrahedral core, four polymeric FUdR oligonucleotides tails and an affibody molecule attached to one end of a polymeric FUdR oligonucleotides tail for targeting HER2. These nanodrugs were prepared by a facile bioconjugation process and DNA self-assembly (Scheme 1A), and had definite drug-loading ratio (19.6%) and stable nanostructure. Then, the potency of nanodrugs was also tested in vitro and in vivo. They exhibited an excellent selectivity and inhibition for HER2-overexpressing breast cancer. Based on the above findings and results, the antibody-like DNA-affibody nanoparticle can be used as a template to design the similar nucleoside nanodrugs for targeting therapy of HER2-overexpressing tumor.

Materials and Methods
Materials and Chemicals
5-Fluorodeoxyuridine was purchased from Alfa Aesar (Shanghai, China). 4,4′-Dimethoxytrityl Chloride (DMT-Cl, 97%) N,N-Diisopropylethylamine (DIPEA, 97%) and
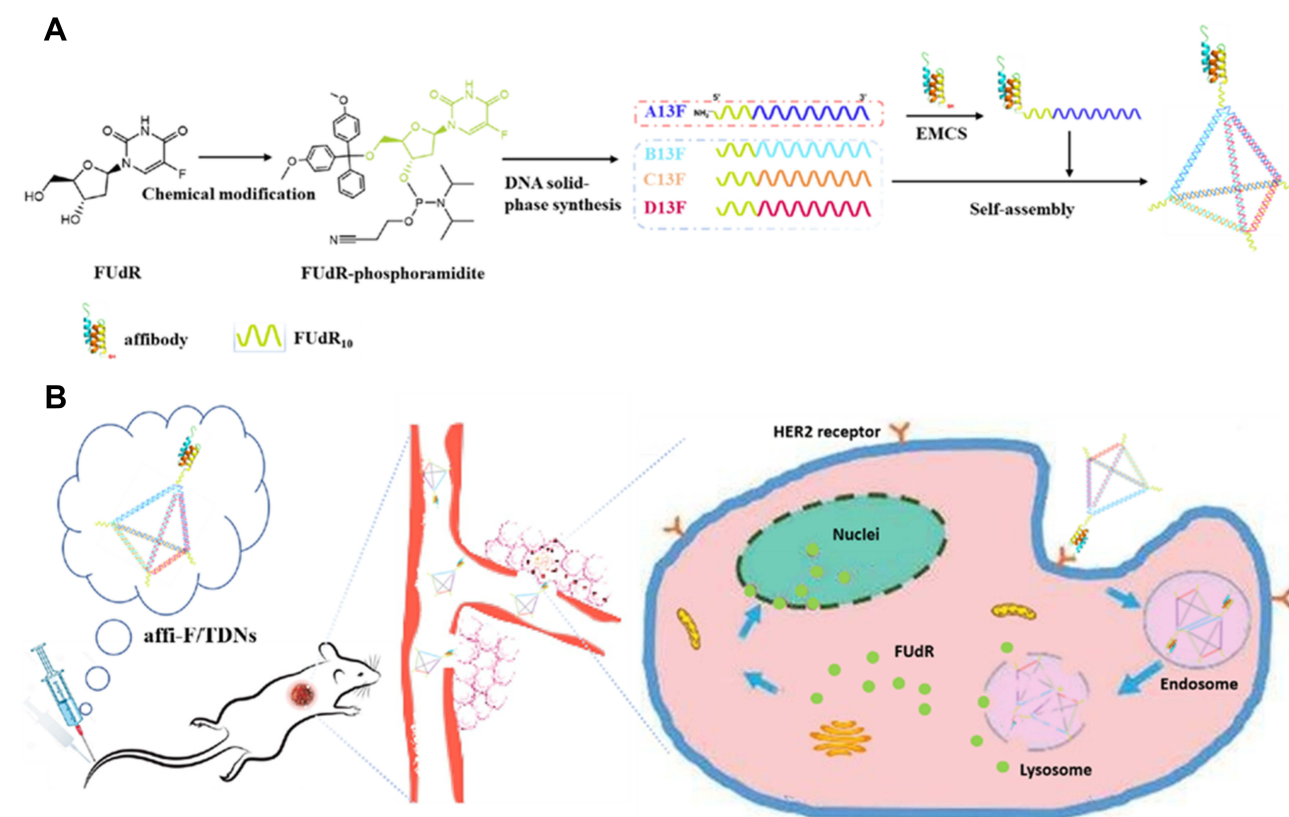
Scheme 1 (**A**) Schematic illustration of preparation procedure of affi-F/TDNs. FUdR was converted into its phosphoramidite and linked to the 5′ end of each DNA strand one by one by solid-phase synthesis. The 5′-NH₂ labeled DNA strand, A13F-NH₂, was conjugated with affibody via EMCS and then self-assembled into affi-F/TDNs with other three DNA strands. (**B**) Schematic illustration of the HER2 receptor-mediated tumor-targeting delivery of affi-F/TDNs in vivo and in vitro. The affi-F/TDNs were injected into blood vessels and accumulated in HER2-overexpressing breast tumor sites. Then, they specifically bound to HER2 receptor on the surface of breast cancer cells and were internalized into cancer cell via receptor-mediated endocytosis. The affi-F/TDNs were degraded in lysosomes by intracellular nucleases to release FUdRs.

2-Cyanoethyl N,N,N',N'-tetraisopropylphosphordiamidite (95%) were obtained from Macklin Inc. (Shanghai, China). N-(ε-malemidocaproyloxy) succinimide ester (EMCS) was purchased from Aladdin (Shanghai, China). Ni-NTA agarose, and Sephadex G-25 were obtained from GE Healthcare (Piscataway, USA). Imidazole, sodium chloride, sodium acetate, polyacrylamide, tris base, acetic acid, ethylenediaminetetraacetic acid (EDTA), magnesium chloride, ethanol, and DAPI were obtained from Sangon Biotech (Shanghai) Co., Ltd (China). Amicon ultracentrifugal filters were purchased from Merck Millipore Ltd (Darmstadt, Germany). RPMI 1640 medium, DMEM medium, MEBM medium, trypsin, 3-(4,5-dimethylthiazol-2-yl)-2,5-diphenyl-2H-tetrazolium bromide (MTT), antibiotic-antimycotic (100×) and fetal bovine serum (FBS) were purchased from Wisent Biotechnology (Nanjing) Co. Ltd (China). All chemicals were used without further purification.

Synthesis of FUdR Phosphoramidite

To integrate FUdR into DNA strands, FUdR was first converted into its corresponding phosphoramidite form, and the detailed synthesis was performed according to a previously reported procedure with slight modification (Scheme S1).[26] In brief, FUdR (2.46 g, 10 mmol) and DMT-Cl (3.38 g, 10.0 mmol) were dissolved in 35 mL of anhydrous pyridine, and stirred at room temperature under a positive pressure of argon for 6 hrs. The reaction mixture was concentrated by rotary evaporator and purified by column chromatography. The obtained FUdR-DMT (2.75 g, 5 mmol) and DIPEA (0.78 g, 6 mmol) were dissolved in 30 mL of anhydrous CH_2Cl_2. Ten milliliters of 2-Cyanoethyl N,N,N',N'-tetraisopropylphosphordiamidite (1.21 g, 5.1 mmol) in anhydrous CH_2Cl_2 was added dropwise to the reaction solution. The reaction was stirred overnight at room temperature under a positive pressure of argon. The reaction mixture was diluted with

50 mL of CH_2Cl_2, washed with saturated brine, and the organic phase was dried over anhydrous Na_2SO_4, filtered, and concentrated by rotary evaporator. Purification by silica gel flash chromatography (discontinuous gradient of ethyl acetate/methanol (1:0–5:1) with 1% triethylamine by volume as eluant) afforded pure product (yield 78%). 1H NMR data of FUdR phosphoramidite follow: ^{1}H NMR (600 MHz, DMSO): δ 11.87 (1H, s), 7.94 (1H, t, J = 6.6 Hz), 7.40 (2H, t, J = 7.2 Hz), 7.32–7.23 (7H, m), 6.88 (4H, J = 8.4 Hz, J =3.0 Hz), 6.17–6.12 (1H, m), 4.54–4.48 (1H, m), 4.06–3.99 (1H, m), 3.74 (3H, s), 3.73 (3H, s), 3.71–3.59 (2H, m), 3.58–3.53 (1H, m), 3.51–3.46 (1H, m), 3.32–3.28 (1H, m), 3.25–3.19 (1H, m), 2.76 (1H, t, J = 11.4 Hz), 2.64 (1H, t, J = 12Hz), 2.44–2.39 (1H, m), 2.37–2.27 (1H, m), 1.13 (3H, J = 6.6 Hz), 1.11–1.09 (6H, m), 0.98 (3H, d, J = 6.6 Hz); ^{13}C NMR (600 MHz, DMSO): δ 158.1, 157.1, 156.9, 148.9, 144.6, 135.3, 135.2, 129.7, 127.8, 127.6, 118.9, 118.7, 113.2, 85.9, 85.8, 84.5, 58.4, 58.2, 55.0, 42.6, 42.5, 24.3, 19.8.

Solid-Phase Synthesis of FUdR-Containing DNA Strands

The synthesis of FUdR-containing DNA strands (FUdR-DNA) was carried out by our laboratory in collaboration with TsingKe Biological Technology. All DNA sequences (listed in Table S1) were synthesized on a Dr. Oligo 96 Oligo Synthesizer (Biolytic Lab Performance, Inc. Fremont, USA) using the standard solid-phase phosphoramidite methodology. The FUdR-DNA strand used to link a targeting ligand was an amino-modified DNA strand, A13F-NH$_2$. After synthesis, the obtained FUdR-DNA strands were cleaved and deprotected from the CPG column, and then precipitated overnight in cold ethanol solution at −20°C. After the supernatant was removed by centrifugation, the FUdR-DNAs were dissolved with 0.1 M triethylamine acetate (TEAA) and purified by reversed phase HPLC using a BioBasic4 column (5 μm, 4.6 x 250 mm, Thermo Fisher Scientific, USA). Finally, the obtained FUdR-DNA strands were characterized by LCMS-2020 (Shimadzu, Japan) and quantified using Nanodrop 2000c (Thermo Fisher Scientific, USA).

Synthesis and Purification of FUdR-DNA-Affibody Chimera

The sequence of the modified affibody molecule Z$_{hcHER2:342}$ used in this study was MIHHHHHHLQVD NKFNKEMRNAYWEIALLPNLNNQQKRAFIRSLYDD-PSQSANLLAEAKKLNDAQAPKVDC.

According to the standard cloning and expression procedures, the modified affibody molecule Z$_{hcHER2:342}$ was expressed in *E. coli* BL21 cells. After the pelleted bacterial cells were harvested and broken, the purified Z$_{hcHER2:342}$ molecules were obtained through affinity chromatography.

The synthesis process of FUdR-DNA-affibody chimera was shown in Scheme S2. The DNA strand A13F-NH$_2$ (261.6 μg, 16.5 nmol) was dissolved in 200 μL of phosphate-buffered saline (PBS) and treated with 20 μL of 50mM EMCS in dimethyl sulfoxide. The reaction mixture was incubated at 37°C for 3 hrs and stopped by the addition of 22 μL of 3 M NaOAc. Next, 600 μL of pre-cooled ethanol was added to the reaction mixture and incubated at −20°C for 30 mins, and then the mixture was centrifuged at 15,000 g for 30 mins. After the resulting precipitate was washed twice with 70% ethanol, it was dissolved in 200 μL of PBS buffer and treated with 1500 μg (180 nmol) affibody in 1000 μL of PBS buffer for 3 hrs at room temperature. Then, the reaction mixture was purified on a Capto DEAE column (1 mL, GE Healthcare), which was eluted with Tris-HCl (10 mM, pH 8.0) buffer containing 0.5–1.0 M NaCl. The purified components were analyzed by 10% native polyacrylamide gel electrophoresis. The gel was run at 100 V for 1 hr and stained with GelStain (Sangon Biotech (Shanghai) Co., Ltd, China). The eluted fraction of the previous step was further purified using a HisTrap HP column (1 mL, GE Healthcare). Finally, the product was eluted with 50 mM Tris-HCl, pH 8.0, containing 300 mM NaCl and 150 mM imidazole. Aliquots of each fraction were analyzed by 10% native polyacrylamide gel electrophoresis. The pure A13F-affibody was concentrated using Amicon ultracentrifugal filters (MW cutoff 10 kDa) and stored at 4°C.

Preparation of Tetrahedral DNA Nanostructures

The sequences of all single-stranded DNAs used to form DNA tetrahedron were shown in Table S1. Four DNA strands, A13 (5 nmol), B13 (5 nmol), C13 (5 nmol) and D13 (5 nmol) were mixed in 2 mL TM buffer (10 mM Tris-HCl, pH 8.0, 12 mM MgCl$_2$). The solution was quickly heated to 95°C for 10 mins, then cooled down to 25°C for 20 mins to form TDNs. Four FUdR-DNA strands, A13F (5 nmol), B13F (5 nmol), C13F (5 nmol) and D13F (5 nmol), were mixed and the FUdR-tetrahedral DNA nanostructures (F/TDNs) were

constructed by the method described above. The affi-F/TDNs were prepared by mixing A13F-affibody (10 nmol), B13F (10 nmol), C13F (10 nmol) and D13F (10 nmol), and the mixture was incubated 75°C for 15 mins. It was then cooled to room temperature. The obtained DNA nanoparticles were analyzed by 10% native polyacrylamide gel electrophoresis. The gel was run at 100 V for 1 hr and stained with GelStain.

Atomic Force Microscopy (AFM) Characterization

For F/TDNs and affi-F/TDNs imaging, 10 µL samples (10 nM) were deposited onto a freshly peeled mica surface for 5 mins. Next, 40 µL of TAE/Mg^{2+} buffer (50 mM Tris, 20 mM acetic acid, 2 mM EDTA, 12 mM MgCl$_2$, pH 8.0) was added in the mica and then dried in air at room temperature. The samples were imaged with AFM (Agilent Technologies, 5500 AFM/SPM System, USA).

Dynamic Light Scattering (DLS)

The hydrodynamic sizes of the affi-F/TDNs were measured with Nanobrook Omni (Brookhaven Instruments Corporation, USA). The concentration of samples used for the DLS analysis was 500 nM.

Stability Analysis of Affi-F/TDNs

Solutions of affi-F/TDNs and single-strand FUdR-DNA (unified to100 µg/mL) were separately mixed with non-heat-inactivated FBS of equal volume and incubated at 37°C. After incubation of 0, 1, 2, 4, and 8 hrs, the mixtures were run on a 10% native polyacrylamide gel electrophoresis and stained with GelStain.

In vitro Release Study of FUdR from Affi-F/TDNs

In order to prove that FUdR can be successfully released from affi-F/TDNs in cells, a simulated enzymatic release test was carried out in vitro. DNase II is widely found inside the animal cells rather than plasma as an acid endonuclease. Thus, affi-F/TDNs were incubated with DNase II at a concentration of 20 U/mL with 8 hrs in acetate buffer (pH 4.5) at 37°C.

Cell Cultures

BT474 breast cancer cells (ATCC HTB-20, overexpression of HER2) were cultured in RPMI-1640 culture medium with FBS and penicillin-streptomycin solution at the concentration of 10% (v/v) and 1% (v/v), respectively. MCF-7 breast cancer cells (ATCC HTB-22, low expression of HER2) were cultured in DMEM containing 10% (v/v) FBS and 1% (v/v) penicillin-streptomycin solution. The human breast epithelial MCF10A cells were cultured in MEBM with 10% (v/v) FBS, 20 ng/mL human epidermal growth factor (EGF), 100 ng/mL cholera toxin, 0.01 mg/mL bovine insulin, and 500 ng/mL hydrocortisone. The cells were placed at 37°C in a humidified atmosphere containing 5% CO$_2$.

Targeted Uptake Evaluation by Confocal Laser Scanning Microscopy

BT474 (1x10^5 cells/well) and MCF-7 cells (1x10^5 cells/well) were separately planted into glass bottom microwell disks at 37°C. When the cell confluency reached about 70%, the cells were treated with FAM-B13F, F/TDNs, and affi-F/TDNs (equivalent to 5 µM FAM), respectively, for 1 hr. The culture solution was carefully removed and the cells were washed 3 times with ice-cold PBS. Thereafter, the cells were fixed with 4% formaldehyde for 20 mins at room temperature and washed 3 times with ice-cold PBS again. Finally, the cell nuclei were stained using 2.5 µg/mL DAPI for 30 mins at 37°C, followed by rinsed with PBS for 2 times. The fluorescent images were obtained using a Zeiss laser scanning confocal microscope (Zeiss LSM 810, Germany). All images were recorded and the target cells were counted using a 40× oil objective.

Targeted Uptake Evaluation by Flow Cytometry

BT474 (1×10^5 cells/well) and MCF-7 cells (1×10^5 cells/well) were seeded in glass bottom microwell disks in 2 mL of medium with 10% FBS for 24 hrs under a humidified 5% CO$_2$ atmosphere at 37°C, respectively. Afterward, the medium was removed carefully and the cells were washed twice with PBS. FAM-B13F, F/TDNs, and affi-F/TDNs (equivalent to 5 µM FAM) were added to the culture medium separately, and the cells were treated for 2 hrs. Subsequently, the medium was removed and the cells were washed with PBS three times. The cells were digested with 0.05% trypsin-EDTA and harvested by centrifugation. The flow cytometry was performed on a BD FACS Calibur (BD, Franklin Lakes, USA). The medium without DNA nanostructures was used as control.

In vitro Cytotoxicity

Exponentially growing BT474, MCF-7, and MCF-10A cells were harvested and plated in 96-well plates at a concentration of 5×10^3 cells/well. After the cells were incubated at 37°C for 24 hrs, the culture medium was replaced with 100 µL of fresh medium containing different concentrations of affibody molecule, TDNs, FUdR, F/TDNs, and affi-F/TDNs, and the cells were incubated for 4 hrs. Then, the cells were washed with PBS thoroughly, and incubated in fresh medium for an additional 72 hrs. Afterward, 10 µL of MTT (5 mg/mL) were added to each well and the plates were incubated at 37°C for 4 hrs. The supernatant was discarded, and 100 µL of DMSO was added to each well. The absorbance was determined at 490 nm. The cell viability was expressed as the percentage of viable cells relative to the PBS-treated control group. Data were reported as the mean of three independent experiments.

Apoptosis Analysis by Flow Cytometry

The cell apoptosis was evaluated by flow cytometry analysis using Annexin V-FITC/PI apoptosis analysis kit (Absin, Shanghai, China) according to the manufacturer's instruction. Briefly, BT474, MCF-7, and MCF-10A cells were seed in six-well plates and allowed to grow for 24 hrs, then exposed to a medium containing free FUdR, F/TDNs, and affi-F/TDNs (a dose equal to 10 µM FUdR) with a subsequent 12 hrs incubation. The cells were subjected to apoptosis analysis using flow cytometry. Both early apoptotic (Annexin V-FITC$^+$/PI$^-$) and late apoptotic (Annexin V-FITC$^+$/PI$^+$) cells were included in cell apoptosis determinations.

Animal Models

All animal procedures were performed in accordance with the Guidelines of the Care and Use of Laboratory Animals at Hebei University and experiments were approved by the Animal Ethics Committee of Hebei University. In order to construct a xenograft model, female NOD/SCID (Mus Musculus) mice, 4–6 weeks old, were purchased from Beijing Vital River Laboratory Animal Technology Co., Ltd. (China), and continued to be fed until their body weight reached about 20 g. BT474 cells (1×10^8 cells) were injected subcutaneously into the right coastal region of mice to establish the tumor model.

In vivo Biodistribution Study

The tumor-targeting ability of affi-F/TDNs was assessed on the BT474 tumor xenograft mouse model. When the tumor size reached about 500 mm^3, 100 µL of 20 µM Cy5.0 labeled F/TDNs and affi-F/TDNs were injected into mice by tail vein injection, respectively. The fluorescence signals were recorded at 1, 2, 4, 8, and 12 hrs after administration using an IVIS Lumina Series III (PerkinElmer, USA) with excitation at 630 nm and emission at 670 nm. Then, to understand the distribution of affi-F/TDNs in various tissues and organs, the mice treated with affi-F/TDNs were sacrificed, and the tumors and major organs (hearts, livers, spleens, lungs, and kidneys) were excised and imaged with the same system.

In vivo Antitumor Study

After the tumor reached about 100 mm^3, the mice were randomly divided into four groups, and received 0.2 mL of PBS, FUdR, F/TDNs, and affi-F/TDNs containing equivalent FUdR concentration (a dose of 10 mg/kg bw) via tail vein injection. The nanodrugs were injected once every 3 days and three times in a row. The tumor volumes and body weights of the mice were monitored and recorded every 3 days. The tumor volume was calculated according to the formula: $V(mm^3) = (length \times width^2)/2$. On day 27, the mice were sacrificed and the tumors were extracted and weighed. The tumor growth inhibition ratio (IR) and the ratio of tumor weight to body weight (tumor/body weight) were calculated by the following formulas.

$$IR(\%)=(1-T_{RTV}/C_{RTV})*100\%, RTV = V_t/V_0$$

$$Tumor/body\ weight = W_{tumor}/W_{body}$$

where T_{RTV} and C_{RTV} were defined as the mean value of the relative tumor volume (RTV) of the test group and the mean value of RTV of the control group, V_0 and V_t were defined as the tumor volume on day 0 and the day that the value was recorded, and W_{tumor} and W_{body} were defined as weight of tumor and mice after the experiment, respectively. Then, the collected tumors and major organs of mice were fixed with 4% paraformaldehyde and cut into 5 µm thick slices for hematoxylin-eosin (HE) staining.

Statistical Analysis

All samples were prepared and tested in triplicates or more. Data were presented as mean ± standard deviation (SD). The statistical significance of differences between groups was determined by the Newman-Keuls analysis. The differences were considered significant for *P<0.05, and highly significant for **P<0.01 and extremely significant for ***P<0.001.

Results and Discussion
Preparation of FUdR-DNA Strands for DNA Tetrahedron Nanoparticle

For delivering the cytotoxic anticancer drug FUdR, DNA tetrahedron nanoparticle was selected as the drug carrier in our study. Four FUdR-DNA strands were synthesized for formation of DNA tetrahedron according to the principle of base pairing. Considering the influence of the addition of FUdR on DNA tetrahedron formation, the DNA strand was screened and optimized. Finally, four 41-mer DNA strands (A13, B13, C13, and D13) were selected to construct DNA tetrahedron with 13 bp in each edge. The DNA sequences information was listed in Table S1. To realize the construction of FUdR-DNA strand, FUdR was derivatized to its phosphoramidite form (Figures S2 and S3), and then linked to the 5′ end of each 41mer DNA strand one by one by solid-phase synthesis. The new four FUdR-DNA strands (A13F, B13F, C13F, and D13F) were characterized by mass spectrometry. The results showed that the measured molecular weights were consistent with the theoretical values (Figure S4, Table S2). It was also confirmed by denatured polyacrylamide gel electrophoresis (PAGE) that FUdR-containing DNA strands were apparently less mobile than unmodified DNA strands (Figure S5). It was also a proof to illustrate FUdRs were successfully inserted into the DNA strands. Furthermore, drug loading with covalent conjugation between FUdRs and DNA strands is more stable and controllable by accurate calculation and solid-phase synthesis process.

Synthesis and Characterization of FUdR-DNA-Affibody Chimera

In order to establish the targeting of DNA nanoparticles, we adopted affibody molecule and connected it to the end of FUdR-DNA strand. The affibody molecule $Z_{HER2:342}$, which was derived from the immunoglobulin G protein Z-domain scaffold, is a small protein with the molecular weight of ~7.0 kDa, and specifically recognizes and binds HER2 receptor on the cancer cell surface (Figure 1A).[27,28] $Z_{hcHER2:342}$ was generated by introducing a cysteine at the C-terminus of $Z_{HER2: 342}$ to provide a thiol group and by fusing with his-tag at its N-terminus for purification by affinity chromatography (Figure 1B and S6). The modified affibody molecule was linked to FUdR at 5′ end of A13F-NH$_2$ through a linker EMCS according to Scheme S2. The A13F-affibody were obtained by two-step purification (Capto DEAE column chromatography and HisTrap HP column chromatography) to remove the

excess affibody molecule and unreacted FUdR-DNA strands, respectively (Figures S7 and S8). UV-vis spectroscopy was used to verify the conjugation of affibody molecule to FUdR-DNA strand via the measurement of the absorbance between 220 nm and 300 nm. Figure 1C shows that the absorption spectrum of A13F-affibody was significantly different from single affibody molecule and FUdR-DNA strand. A13F-affibody was identified by SDS-PAGE, and the gel was treated with GelRed and Coomassie Brilliant Blue R250, which stained the DNA and protein, respectively (Figure 1D). These results suggested that DNA strand and affibody molecule were coupled and pure FUdR-DNA-affibody chimeras were obtained by efficient purification process.

Preparation and Characterization of Self-Assembled Affi/F-TDNs

The obtained FUdR-DNA-affibody chimera (A13F-affibody) was mixed with other three single strands (B13F, C13F, and D13F) in an equimolar amount, and self-assembled into affi-F/TDNs (Scheme 1A). Each edge of the tetrahedron consists of 13 base pairs and each vertex connects 10 FUdR molecules. An affibody molecule is linked to one vertex of the tetrahedron through polymeric FUdR. As a comparison, TDNs were constructed using the above method. The obtained nanoparticles were characterized by 10% native PAGE. As shown in Figure 2A, a prominent band appeared in each DNA nanoparticle, and their mobility apparently decreased along with the drug modification and bioconjugation with affibody. The hydrodynamic size of affi-F/TDNs was 23.27±0.85 nm as determined by dynamic light scattering (DLS) (Figure 2B). Furthermore, affi/F-TDNs were characterized by atomic force microscopy (AFM) and showed about 20 nm length and 3.76 (±0.39) nm height at the dried state, which was larger than F/TDNs (about 15 nm length) (Figures 2C and S9). These results demonstrated that affi-F/TDNs were constructed by self-assembly without influence of polymeric FUdR tails and affibody. In addition, 19.6% of FUdR in molar ratio was loaded in affi/F-TDNs, which was higher than that of the DNA polyhedron (18.3%).[21] Moreover, as targeted nanodrug, each affi-F/TDNs was conjugated with 40 drug molecules, far more than the antibody-drug-conjugate (ADC) drug-loading capacity (typically an average of 3–4 payloads per antibody).[29] The test of stability of affi-F/TDNs was also conducted under physiological conditions. The nanodrugs were incubated with 50% non-inactivated fetal bovine serum (FBS).
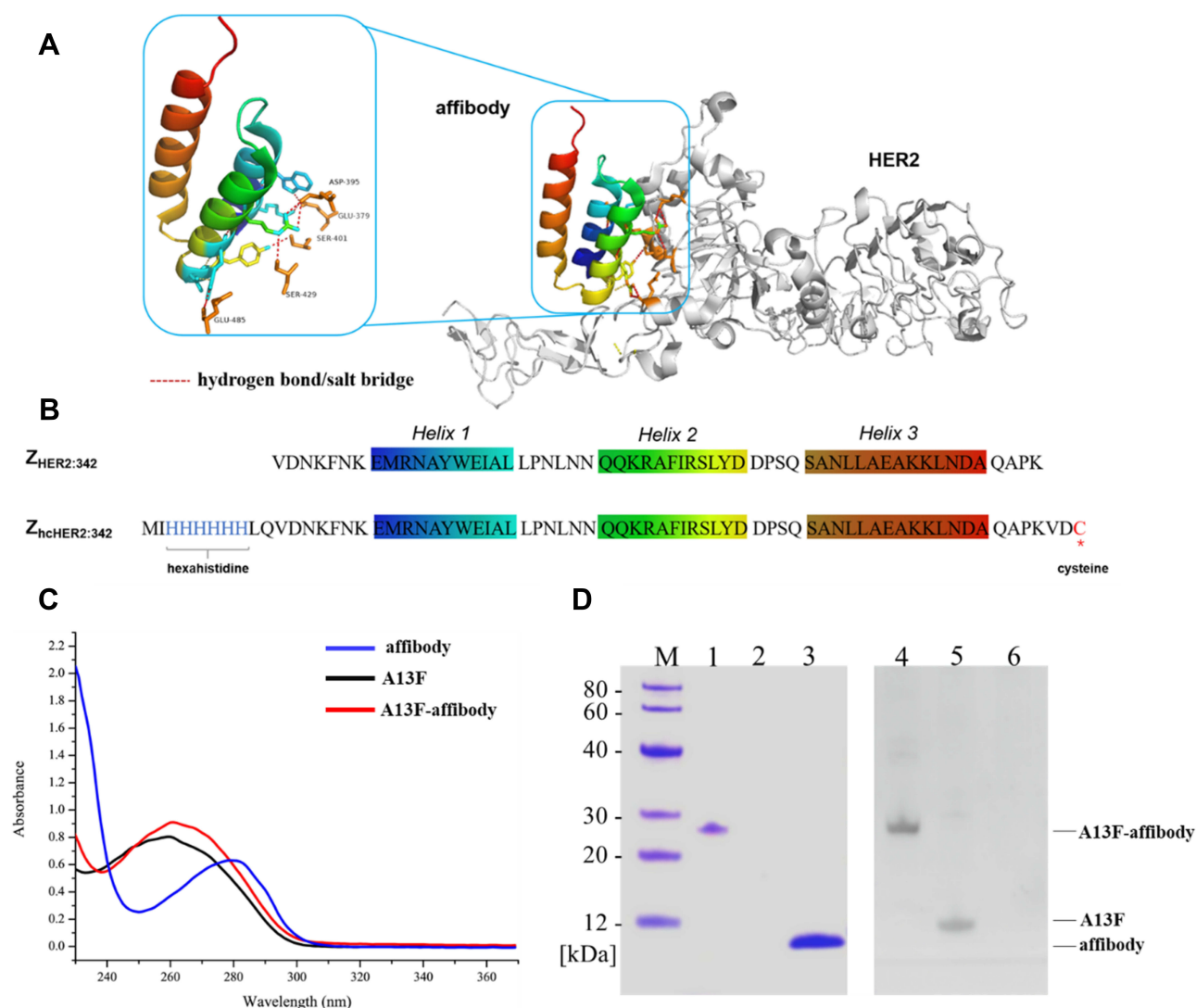
Figure 1 (**A**) 3D structure of affibody molecule $Z_{HER2:342}$-HER2 complex. Affibody is composed of three α-helices and bind to HER2 receptor through hydrogen bond/salt bridge. (**B**) The amino acid sequence of $Z_{HER2:342}$ and $Z_{hcHER2:342}$. The hexahistidine tag of $Z_{hcHER2:342}$ was colored blue, and cysteine residue of $Z_{hcHER2:342}$ was colored red. (**C**) Characterization of purified A13F-affibody via UV-vis spectroscopy. (**D**) Characterization of purified A13F-affibody by SDS-PAGE. The gel was stained by Coomassie Brilliant Blue R-250. Lane M, protein Marker; Lane 1, A13F-affibody; lane 2, DNA strand A13F; lane 3, affibody; The gel stained with GelStain. Lane 4, A13F-affibody; lane 5, DNA strand A13F; lane 6, affibody.

When they were incubated at 37°C for 4 hrs, no obvious change was observed by gel electrophoresis (Figure S10), indicating that they were stable in FBS. In contrast, single-stranded DNA was almost completely degraded by the nuclease in FBS when incubated for only 2 hrs. Therefore, these results confirmed that the affi-F/TDNs can perfectly work as a nanodrug, which retains intact nanoparticles in plasma until it enters cancer cells.

Specific Cellular Uptake of Affi-F/TDNs

To investigate the targeting efficiency of affi-F/TDNs, breast cancer cells, BT474 (HER2 overexpressing cell line) and MCF-7 (HER2 low expressing cell line)[30] were

employed for cell uptake test by confocal microscopy and flow cytometry after incubated with FAM-labeled DNA nanoparticles. F/TDNs and FUdR-DNA strands were used as the controls for analysis of cell uptake. In BT474 cells, the different uptake capability was observed. A strong green fluorescence appeared after BT474 cells were treated with affi-F/TDNs, whereas the weak fluorescence was captured in BT474 cells treated with F/TDNs and FUdR-DNA strands (Figure 3A). There was a difference of more than 2.0-fold intensity between the strong and weak fluorescence (Figure 3B). It was inferred that affi-F/TDNs had significant targeting ability to HER2-overexpressing cancer cells. This was mainly attributed to the specific binding
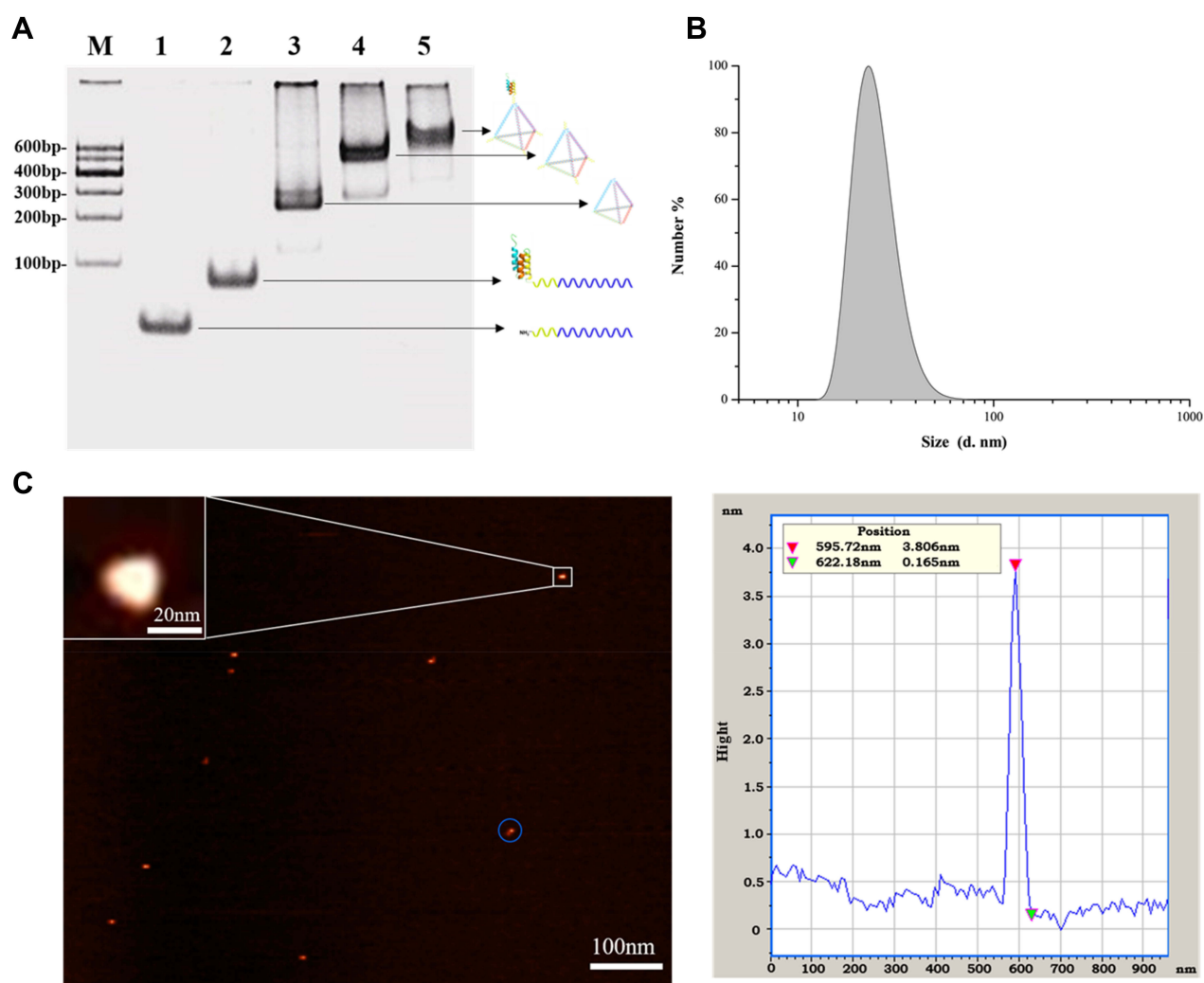
Figure 2 Characterization of DNA nanoparticles. (**A**) Electrophoresis analysis of the self-assembled DNA nanoparticles. Lane M, DNA Marker-B; lane 1, DNA single strand A13F-NH$_2$; lane 2, A13F-affibody; lane 3, TDNs; lane 4, F/TDNs; lane 5, affi-F/TDNs. (**B**) DLS data of affi-F/TDNs. (**C**) AFM image of affi/F-TDNs.

of the affibody to the HER2 receptor through eight hydrogen bonds and six salt bridges (Figure 1A). As illustrated in Scheme 1B, the affi-F/TDNs-HER2 receptor complex was formed on the surface of BT474 cells, which was shown in its fluorescence image. Then, the HER2 receptor-mediated endocytosis enabled cells to absorb extracellular substances. Subsequently, the affi-F/TDNs-HER2 receptor complex was internalized into endosomes and further processed into late endosomes/multivesicular bodies and lysosomes. In this process, affi-F/TDNs were degraded in lysosomes by intracellular nucleases and protease to release FUdR (Figure S11) as the HER2 receptors were recycled to the cell membrane.[31] On the contrary, F/TDNs and FUdR-DNA strands were not efficiently absorbed by BT474 cells due to the lack of affibody in their structures.[32,33] When affi-F/TDNs acted on MCF-7

(HER2 low expressing cell line) instead of BT474 cells, a relatively weak fluorescence was detected, which was suggested that the ability of affi-F/TDNs to bind to HER2 low expressing cancer cells was inferior to that of HER2-overexpressing cancer cells. The flow cytometry results further demonstrated that affi-F/TDNs had excellent targeting ability and high specificity for BT474 cells (Figure 3C). This targeted nanodrug is of potential for future application in preventing rapid metabolism of FUdR in plasma and reducing toxicity to healthy tissue.

In vitro Cytotoxicity of Affi-F/TDNs
MTT assay was taken to assess the potential cytotoxicity of affi-F/TDNs. As a blank test, affibody molecule and TDNs did not show any cytotoxicity in normal (MCF-10A) and tumor (BT474 and MCF-7) cells with a wide
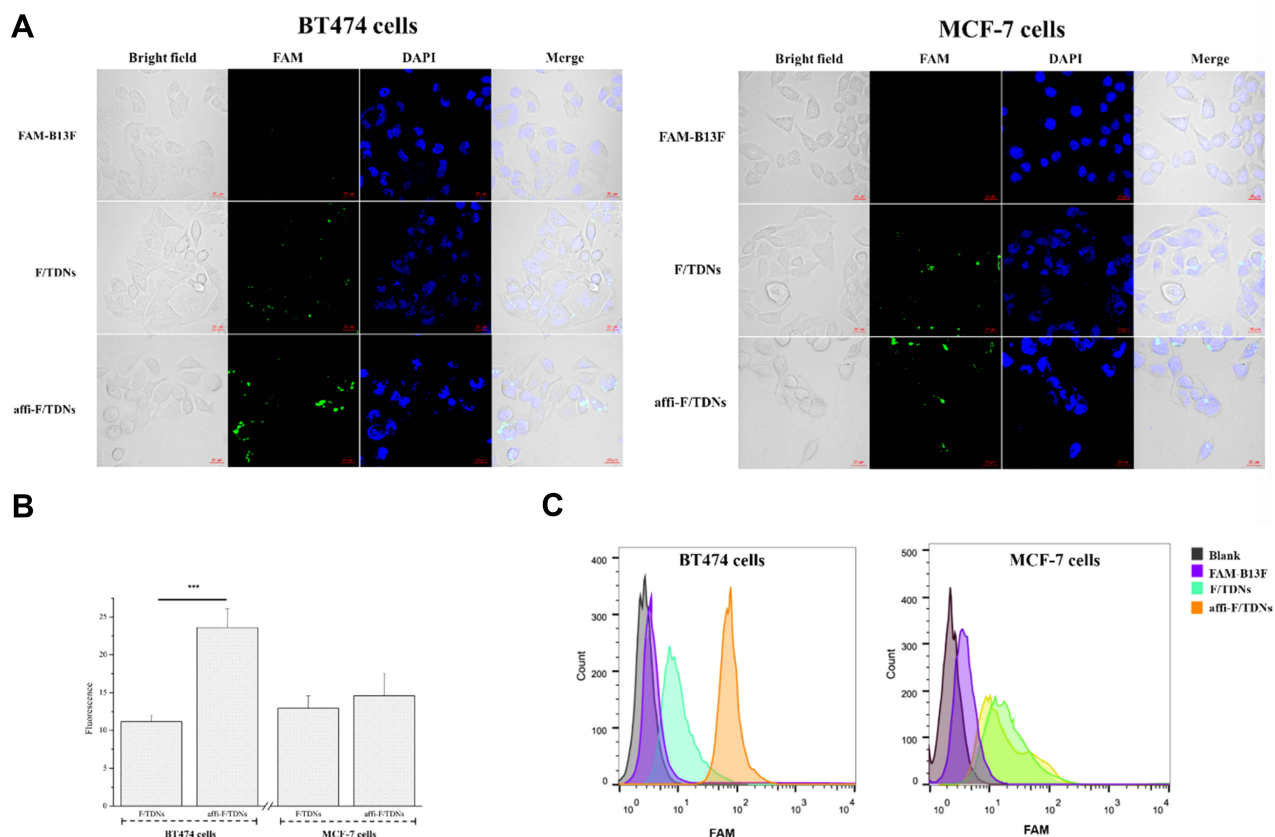
Figure 3 The cellular uptakes of DNA nanoparticles. (**A**) Confocal laser scanning microscopy of FAM-B13F, F/TDNs, and affi-F/TDNs in BT474 and MCF-7 cells. Scale bar: 20 μm. (**B**) Semi-quantitative analysis of fluorescence intensity. DATA are presented as mean ± SD (n=3). Statistical analysis: ***p<0.001. (**C**) Flow cytometry analysis of cellular uptake of DNA nanoparticles to BT474 and MCF-7 cells.

range of concentrations (50 nM to 1000 nM) (Figure 4A). Based on these findings, it can be assumed that these protein and DNA materials present an adequate biocompatibility and safety for drug delivery. Then, the potential toxicity of affi-F/TDNs as a nanodrug to normal cells was tested, and Figure 4B shows that affi-F/TDNs displayed lower cytotoxicity in MCF-10A than free FUdR and F/TDNs, which may be effective in reducing the side effects of FUdR-based chemotherapy.

Next, Figure 4C exhibits the in vitro cytotoxic effect of affi-F/TDNs, F/TDNs, and free FUdR on BT474 and MCF-7 cells, and it was found that they inhibited cell proliferation in a dose-dependent manner. For BT474 cells, affi-F/TDNs presented the highest cytotoxicity and the cell viability decreased to 18.8%, whereas in the existence of free FUdR and F/TDNs, their cell viability was 61.8% and 39.8%, respectively (Figure 4C). The highest inhibition of affi-F/TDNs may be associated with an enhanced cellular uptake via HER2-mediated endocytosis, thus leading to a significantly enhanced effect against the

HER2-overexpressing cancer cells. Due to the higher cytotoxicity of the polymerized form of FUdR,[34] F/TDNs also displayed a higher inhibitory effect than free FUdR. The lower cytotoxicity of free FUdR may be attributed to the inadequacy of specialized drug transporter proteins and the efflux of drug molecules by P-glycoprotein (P-gp) pumps.[35] Next, the cytotoxicity of affi-F/TDNs to MCF-7 cells was also evaluated by the same method described above. Compared with BT474 cells, affi-F/TDNs caused lower cytotoxicity against MCF-7 cells, which may be due to the decreased drug uptake into the cells with low HER2 expression levels. Based on the above results, it was demonstrated that affi-F/TDNs were effectively transported into HER2-overexpressing cancer cells because of the excellent targeting ability to HER2, resulting in a significantly enhanced antitumor activity.

Cell Apoptosis Assays

As a chemotherapeutic drug, FUdR has been reported capable of inducing cell apoptosis.[36] So, the Annexin V-FITC/
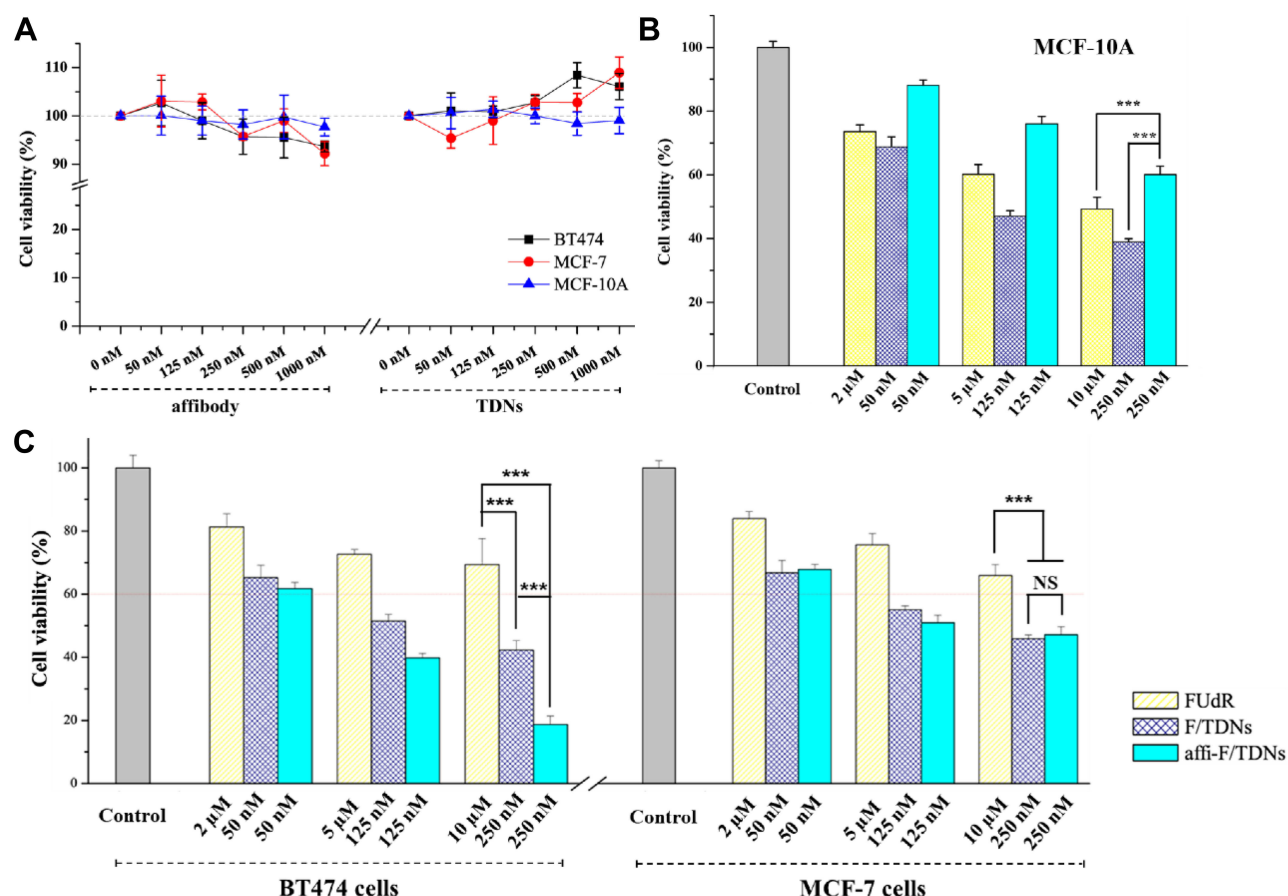
Figure 4 In vitro cytotoxicity assay. (**A**) Cell viability of BT474, MCF-7, and MCF-10A cells incubated with increasing concentrations of affibody molecule and TDNs for 72 hrs. (**B**) Cell viability of MCF-10A cells incubated with FUdR, F/TDNs, and affi-F/TDNs for 72 hrs. (**C**) Cell viability of BT474 and MCF-7 cells incubated with FUdR, F/TDNs, and affi-F/TDNs for 72 hrs. The results are expressed as a percentage of the control group, Data are presented as mean ± SD (n=5). Statistical analysis: ***p<0.001, No significant difference (NS).

propidium iodide (PI) stain was used to measure the affi-F/TDNs induced total apoptosis, including early (Annexin V-FITC$^+$/PI$^-$) and late apoptosis (Annexin V-FITC$^+$/PI$^+$). The breast cancer cells (BT474 and MCF-7) and normal breast cells (MCF-10A) were pretreated with free FUdR, F/TDNs, and affi-F/TDNs for 12 hrs. As shown in flow cytometry (Figure 5A and B), free FUdR and F/TDNs induced a low apoptosis rate in the BT474 cells, whereas a significant increase in the percentage of apoptotic cells was observed in cells treated with affi-F/TDNs (31.9 ± 0.6%), indicating that affi-F/TDNs enhanced apoptosis induction of HER2-overexpressing cancer cells through targeted chemotherapy. By contrast, the apoptosis rate of the affi-F/TDNs treated MCF-7 cells were 14.7±1.5%, which was similar to that of MCF-7 cells treated with F/TDNs. This may be due to affi-F/TDNs have no targeted therapeutic effect on cancer cells with low HER2 expression. It was worth mentioning that affi-F/TDNs induced a lower rate of apoptosis (7.4±1.2%) in MCF-10A cells than that of free FUdR and F/TDNs chemotherapy, thus supporting the lower toxicity of affi-F/TDNs against normal cells.

Targeting of Affi-F/TDNs to Cancer Xenograft in vivo

In order to verify whether affi-F/TDNs still had the targeting ability in vivo, the Cy5.0-labeled nanodrugs were injected into tumor-bearing mice via tail vein and the fluorescence distribution was monitored using an IVIS Lumina Series III. It can be clearly observed from Figure 6A that both affi-F/TDNs and F/TDNs rapidly covered the whole body of the mice at one-hour post-injection. As the blood circulation continued, the distribution of the two nanodrugs in mice showed significant differences. At 4 hrs after injection, the affi-F/TDNs-treated mice had a stronger fluorescent signal at the tumor region compared with F/TDNs-treated mice,
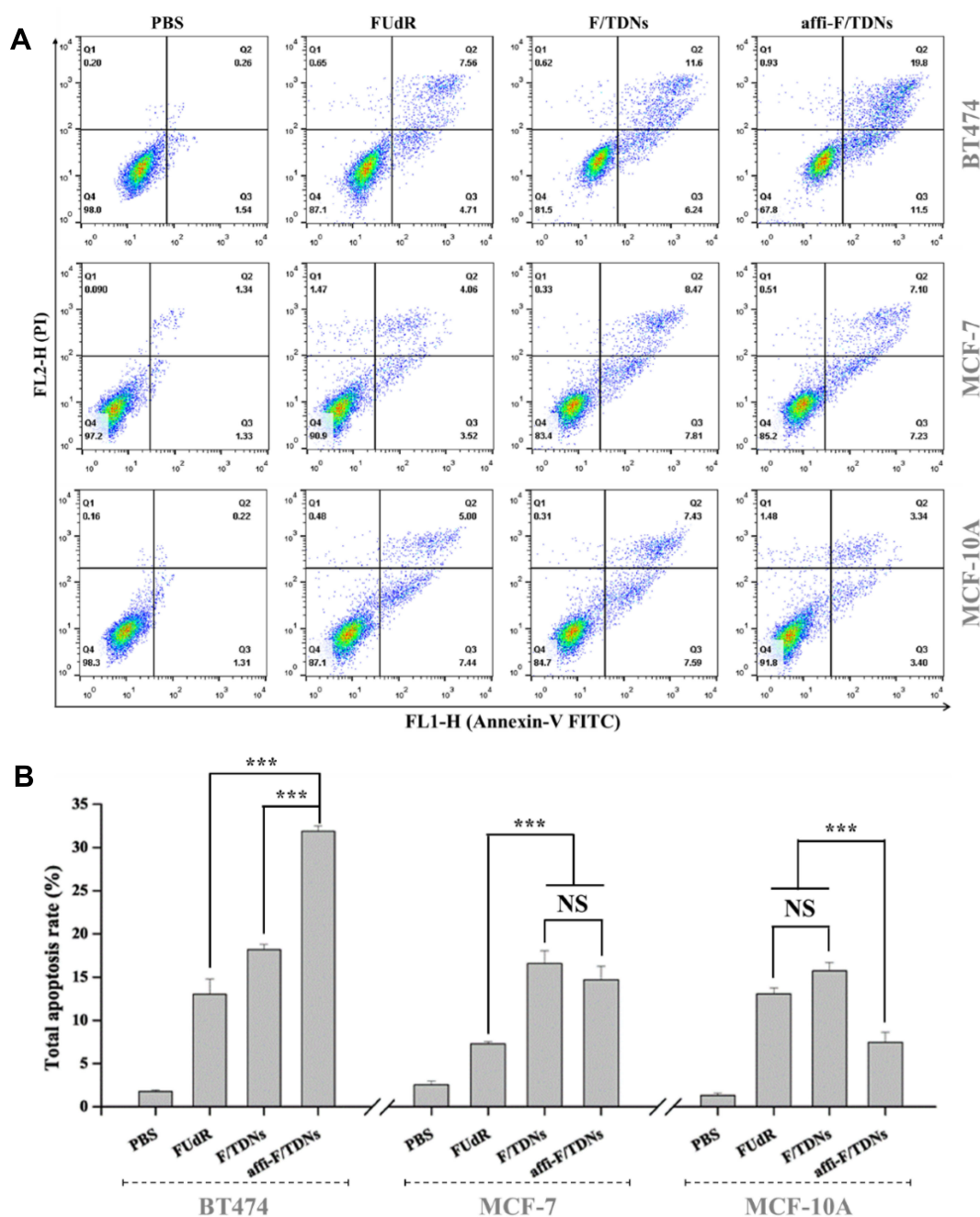
Figure 5 Cell apoptosis assay using flow cytometry. (**A**) Flow cytometry scatterplots of apoptosis rate in BT474, MCF-7 and MCF-10A cells. (**B**) Quantitative analysis of the total apoptosis rate in above cells. Data are presented as mean ± SD (n=3). Statistical analysis: ***p<0.001, no significant difference (NS).

indicating that affi-F/TDNs could largely accumulate in the tumor region. Such differential result might be attributed to the affibody ligand in affi-F/TDNs to potentially inducing specific active transport via the HER2-mediated endocytosis.[30] Furthermore, to investigate the localization of affi-F/TDNs within specific tissue compartments, various organs and tumors were dissected and collected at 1, 2, 4, 8, and 12 hrs. It is

also found from Figure 6B that affi-F/TDNs showed low accumulation in all normal tissues and were rapidly metabolized in a short period of time (about 8 hrs), which might contribute to the low systematic toxicity. It was also noteworthy that affi-F/TDNs were mainly accumulated in tumor tissues and last for more than 12 hrs, which might be helpful to improve the therapeutic effect of FUdR through sustained release.
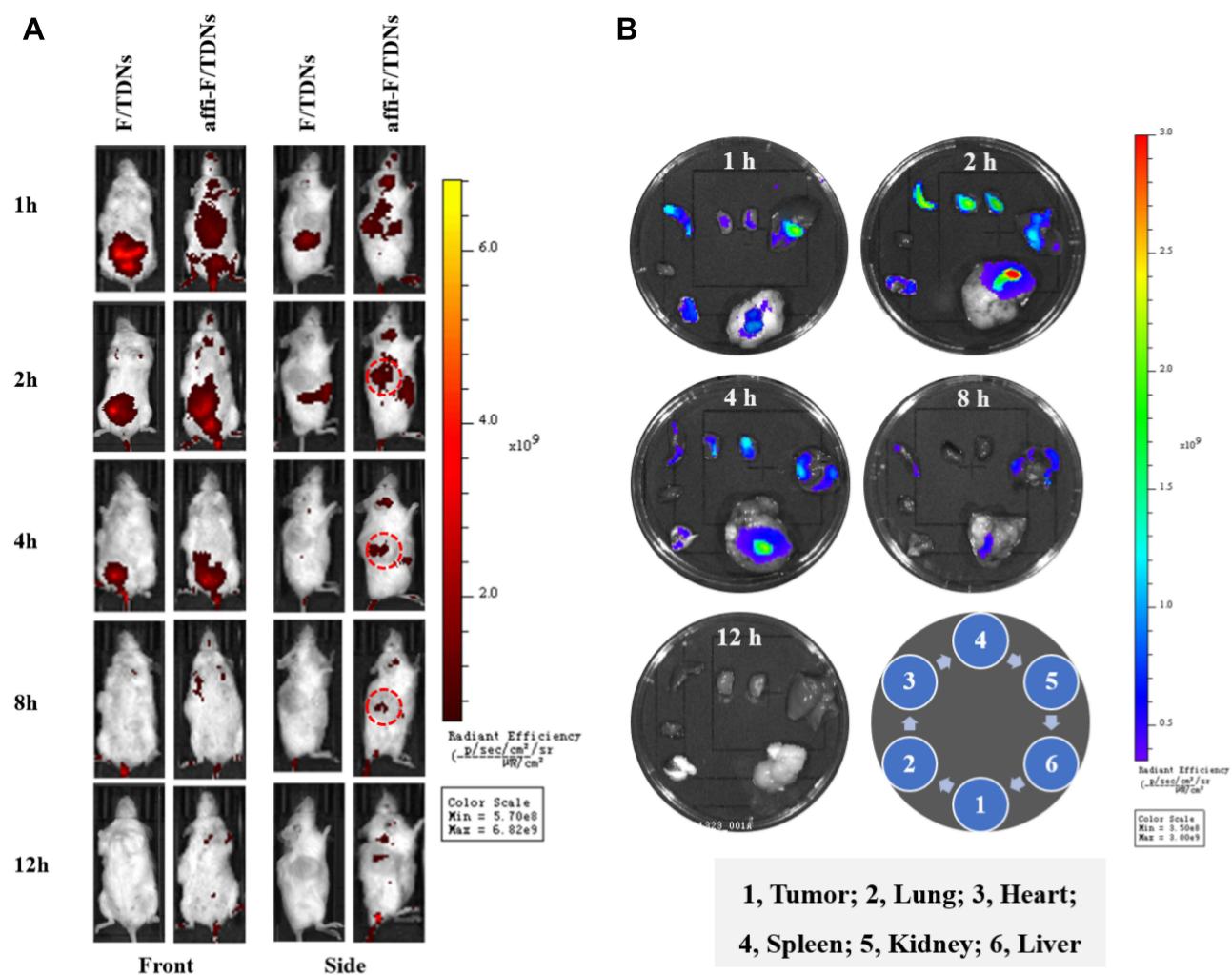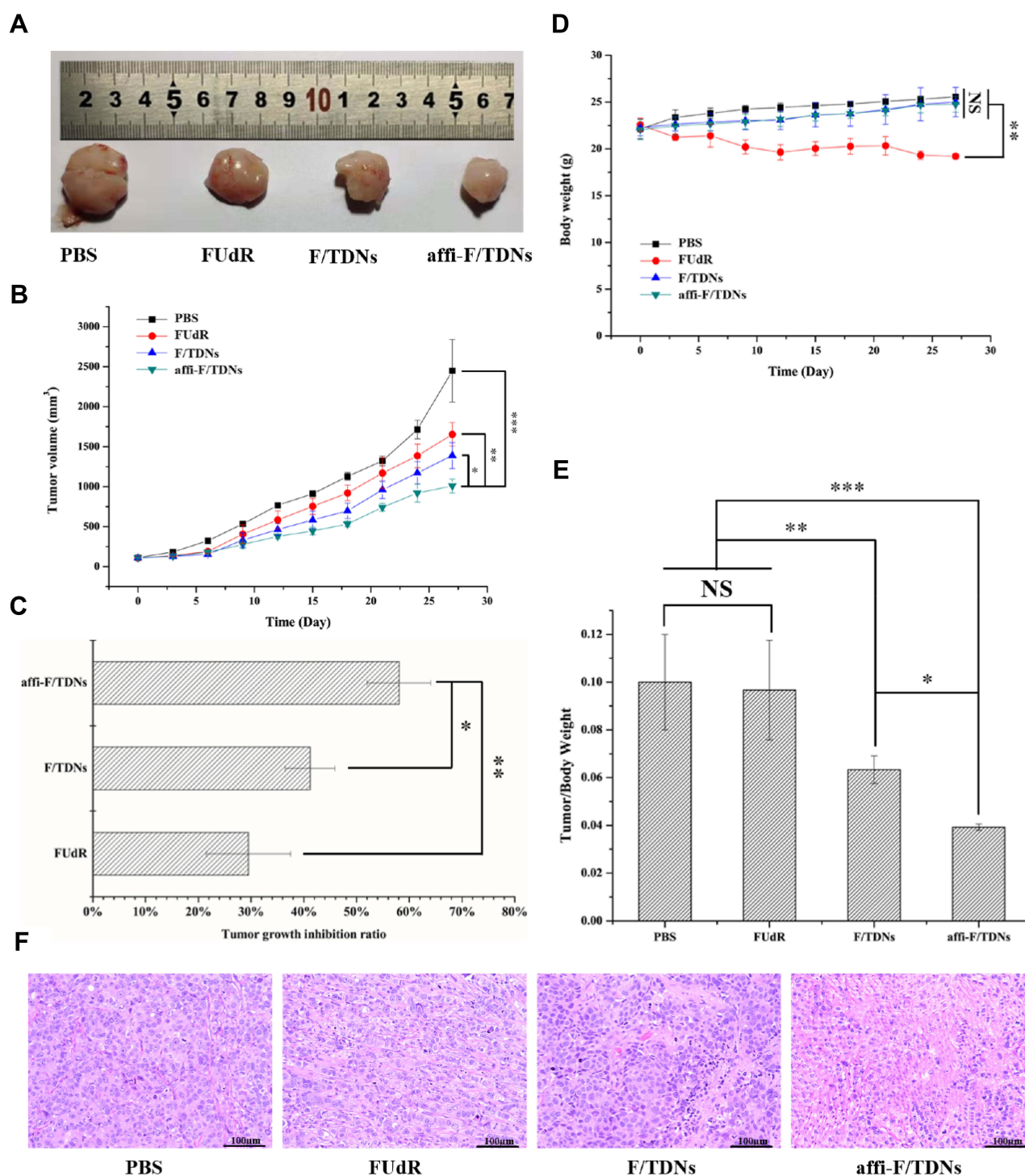
Figure 6 In vivo biodistribution and antitumor effects of affi-F/TDNs on female NOD/SCID (Mus Musculus) mice with BT474 tumor xenograft. (**A**) In vivo fluorescent image of tumor-bearing mice after 12 hrs of intravenous injection of the Cy5.0 labelled F/TDNs and affi-F/TDNs. (**B**) The fluorescence imaging of various tissues (tumors, lungs, hearts, spleens, kidneys, and livers) at 1, 2, 4, 8, and 12 hrs after of intravenous injection of the Cy5.0 labelled affi-F/TDNs.

In vivo Tumor Inhibition by Affi-F/TDNs

Based on the outstanding performance of affi-F/TDNs in vitro, the in vivo antitumor efficacy was evaluated on a female NOD/SCID (Mus Musculus) mice model bearing BT474 tumor xenografts. After three consecutive intravenous injections of the nanodrugs, the tumor growth and body weight were recorded every 3 days during the treatment. As shown in Figure 7A–C, compared with the free FUdR treatment group, both F/TDNs and affi-F/TDNs groups exhibited more significant growth inhibitory effects. These results once again proved that DNA nanoparticles integrated with FUdRs could achieve the enhanced antitumor efficacy. Interestingly, affi-F/TDNs were proved to be a more efficient nanodrug with an inhibition ratio (IR) of 58.1% compared with F/TDNs (IR, 41.2%), and this excellent

antitumor effect might be due to the specific binding and internalization of tumor cells mediated by the overexpressed HER2. In addition, the body weights of mice were monitored to evaluate the systemic toxicities of the treatments. The monitoring results (Figure 7D) showed that the bodyweight of mice in the F/TDNs and affi-F/TDNs treatment groups increased slightly during the treatment process, implying their low systemic toxicities. However, the weight of free FUdR treatment group was significantly reduced, which may be related to the strong toxic and side effects of FUdR. The data of tumor/body weight (Figure 7E) also confirmed the above results. Finally, H&E staining was used for pathological examination of tumors and various tissues and organs. As shown in Figure 7F, the tumor sections in the group treated with affi-F/TDNs exhibited more severe cancer

Figure 7 In vivo antitumor effects of affi-F/TDNs on female NOD/SCID (Mus Musculus) mice with BT474 tumor xenograft. (**A**) Images of resected tumors. (**B**) Tumor volumes of each group during the whole treatment. (**C**) Tumor growth inhibition ratio (IR). (**D**) Bodyweight changes (**E**) Tumor/bodyweight of mice after the end of study. Data represent as mean± SD (n=6). Statistical analysis: *p<0.05, **p<0.01, ***p<0.001, no significant difference (NS). (**F**) Histological images of BT474 tumor slices treated with PBS, FUdR, F/TDNs, and affi-F/TDNs after staining with H&E (magnification 200×).

necrosis and a lower nuclear-to-cytoplasmic ratio than the other groups. Meanwhile, no obvious abnormality was observed in the major organs of mice treated with PBS and affi-F/TDNs (Figure S12). Therefore, these results demonstrated that the DNA-based nanodrugs had very good treatment effect and low systemic toxicity.

Conclusions

In summary, a new affibody-DNA tetrahedron template was successfully constructed for loading nucleoside analogue FUdR. This DNA nano-structure had a very high drug-loading ratio, and the amount of FUdR can be accurately controlled. In addition, the affi-F/TDNs exhibited good stability and entered cancer cells with intact nanoparticles. Then, FUdRs were sustained-released by degradation of nuclease in cancer cells. The in vitro and in vivo results demonstrated that the affi-F/TDNs had a capability of specifically targeting HER2-overexpressing breast cancer cells and displayed excellent anticancer efficacy, which promoted the pre-clinical application of the nanodrug. Furthermore, the affibody-DNA tetrahedrons as a platform facilitates efficient loading of many other nucleoside analogues, such as gemcitabine, decitabine and clofarabine, and utilizing other types of affibody molecules as targeting ligand for this nanocarrier will further expand the cancer therapeutic range.

Ethics Approval and Consent to Participate

All animal experiments were carried out in compliance with the Animal Management Rules of the Ministry of Health of the People's Republic of China (Document No. 552001) and the guidelines for Care and Use of Laboratory Animals of Hebei University.

Acknowledgments

Disclosure

The authors report no conflicts of interest in this work.

References

1. Freddie B, Jacques F, Isabelle S, Rebecca LS, Lindsey AT, Ahmedin J. Global cancer statistics 2018: GLOBOCAN estimates of incidence and mortality worldwide for 36 cancers in 185 countries. *CA Cancer J Clin*. 2018;68:394–424. doi:doi:10.3322/caac.21492

2. Slamon DJ, Godolphin W, Jones LA, et al. Studies of the HER-2/neu proto-oncogene in human breast and ovarian cancer. *Science*. 1989;244:707–712. doi:10.3109/07357909009017573

3. Amodio R, Zarcone M, Cusimano R, et al. Target therapy in HER2-overexpressing breast cancer patients. *OMICS*. 2011;15:363–367. doi:10.1089/omi.2010.0125

4. Slamon DJ, Leyland-Jones B, Shak S, et al. Use of chemotherapy plus a monoclonal antibody against HER2 for metastatic breast cancer that overexpresses HER2. *N Engl J Med*. 2001;344:783–792. doi:10.1056/NEJM200103153441101

5. Seidman AD, Berry D, Cirrincione C, et al. Randomized Phase III trial of weekly compared with every-3-weeks paclitaxel for metastatic breast cancer, with trastuzumab for all HER-2 overexpressors and random assignment to trastuzumab or not in HER-2 nonoverexpressors: final results of cancer and leukemia group B protocol 9840. *J Clin Oncol*. 2008;26:1642–1649. doi:10.1200/JCO.2007.11.6699

6. Whitehead TA. A peptide mimic of an antibody. *Science*. 2017;358:450–451. doi:10.1126/science.aap9608

7. Ståhl S, Gräslund T, Karlström AE, Frejd FY, Löfblom J. Affibody molecules in biotechnological and medical applications. *Trends Biotechnol*. 2017;35:691–712. doi:10.1016/j.tibtech.2017.04.007

8. Mehra R, Burtness B. Antibody therapy for early-stage breast cancer: trastuzumab adjuvant and neoadjuvant trials. *Expert Opin Biol Ther*. 2006;6:951–962. doi:10.1517/14712598.6.9.951

9. Davoli A, Hocevar BA, Brown TL. Progression and treatment of HER2-positive breast cancer. *Cancer Chemother Pharmacol*. 2010;65:611–623. doi:10.1007/s00280-009-1208-1

10. Vanderhoeven F, LR A, Martinez AL, Vargas-Roig LM, Sanchez AM, Flamini MI. Synergistic antitumor activity by combining trastuzumab with retinoic acid in HER2 positive human breast cancer cells. *Oncotarget*. 2018;9:26527–26542. doi:10.18632/oncotarget.25480

11. Kim KS, Kim JY, Kim DH, Hwang HS, Na K. Multifunctional trastuzumab-chlorin e6 conjugate for treatment of HER2-positive human breast cancer. *Biomater Sci*. 2018;6:1217–1226. doi:10.1039/c7bm01084b

12. Buzdar AU, Valero V, Ibrahim NK, et al. Neoadjuvant therapy with paclitaxel followed by 5-fluorouracil, epirubicin, and cyclophosphamide chemotherapy and concurrent trastuzumab in human epidermal growth factor receptor 2-positive operable breast cancer: an update of the initial randomized study population and data of additional patients treated with the same regimen. *Clin Cancer Res*. 2007;13:228–233. doi:10.1158/1078-0432.ccr-06-1345

13. Smith I, Procter M, Gelber RD, et al. HERA study team. 2-year follow-up of trastuzumab after adjuvant chemotherapy in HER2-positive breast cancer: a randomized controlled trial. *Lancet*. 2007;369:29–36. doi:10.1016/S0140-6736(07)60028-2

14. Romond EH, Perez EA, Bryant J, et al. Trastuzumab plus adjuvant chemotherapy for operable HER2-positive breast cancer. *N Engl J Med*. 2005;353:1673–1684. doi:10.1056/NEJMoa052122

15. Longley DB, Harkin DP, Johnston PG. 5-fluorouracil: mechanisms of action and clinical strategies. *Nat Rev Cancer*. 2003;3:330–338. doi:10.1038/nrc1074

16. Seo HW, Kim DY, Kwon DY, et al. Injectable intratumoral hydrogel as 5-fluorouracil drug depot. *Biomaterials*. 2013;34:2748–2757. doi:10.1016/j.biomaterials.2013.01.006

17. Elmeshad AN, Mortazavi SM, Mozafari MR. Formulation and characterization of nanoliposomal 5-fluorouracil for cancer nanotherapy. *J Liposome Res*. 2014;24:1–9. doi:10.3109/08982104.2013.810644

18. Roth SK, Epley CC, Novak JJ, Mcandrew ML, Jie Z, Dawn CH. Photo-triggered release of 5-fluorouracil from a MOF drug delivery vehicle. *Chem Commun*. 2018;54:7617–7620. doi:10.1039/C8CC01601A

19. Shayan K, Nowroozi A. Boron nitride nanotubes for delivery of 5-fluorouracil as anticancer drug: a theoretical study. *Appl Surf Sci*. 2018;428:500–513. doi:10.1016/j.apsusc.2017.09.121

20. Wang P, Meyer TA, Pan V, Dutta PK, Ke Y. The beauty and utility of DNA origami. *Chem*. 2017;2:359–382. doi:10.1016/j.chempr.2017.02.009

21. Mou Q, Ma Y, Pan G, Xue B, Zhu X. DNA trojan horses: the self-assembled floxuridine-containing DNA polyhedra for cancer therapy. *Angew Chem Int Ed*. 2017;129:12528–12532. doi:10.1002/ange.201706301

22. Jorge AF, Aviñó A, Pais AACC, Eritja R, Fàbrega C. DNA-based nanoscaffolds as vehicles for 5-fluoro-2′-deoxyuridine oligomers in colorectal cancer therapy. *Nanoscale*. 2018;10:7238–7249. doi:10.1039/C7NR08442K

23. Zhang Y, Jiang S, Zhang D, Bai X, Hecht SM, Chen SX. DNA-affibody nanoparticles for inhibiting breast cancer cells overexpressing HER2. *Chem Commun*. 2017;53:573–576. doi:10.1039/c6cc08495h

24. Zhang C, Zhang HL, Han MN, Yang XL, Li W, Chen SX. DNA-affibody nanoparticle delivery system for cisplatin-based breast cancer chemotherapy. *RSC Adv*. 2019;9:1982–1989. doi:10.1039/C8RA08735K

25. Silva EF, Bazoni RF, Ramos EB, Rocha MS. DNA-doxorubicin interaction: new insights and peculiarities. *Biopolymers*. 2016;107:22998–23007. doi:10.1002/bip.22998

26. Marasco CJJ, Sufrin JR. A convenient method for the direct incorporation of 5-fluoro-2′- deoxycytidine into oligodeoxynucleotides. *J Org Chem*. 1992;57:6363–6365. doi:10.1021/jo00049a061

27. Lee SB, Hassan M, Fisher R, et al. Affibody molecules for in vivo characterization of HER2-positive tumors by near-infrared imaging. *Clin Cancer Res*. 2008;14:3840–3849. doi:10.1158/1078-0432.CCR-07-4076

28. Eigenbrot C, Ultsch M, Dubnovitsky A, Abrahmsen L, Hard T. Structural basis for high-affinity HER2 receptor binding by an engineered protein. *Proc Natl Acad Sci USA*. 2010;107:15039–15044. doi:10.1073/pnas.1005025107

29. Lambert JM, Morris CQ. Antibody-drug conjugates (ADCs) for personalized treatment of solid tumors: a review. *Adv Ther*. 2017;34:1015–1035. doi:10.1007/s12325-017-0519-6

30. Zielinski R, Lyakhov I, Jacobs A, et al. Affitoxin-a novel recombinant, HER2-specific, anticancer agent for targeted therapy of HER2-positive tumors. *J Immunother (1991)*. 2009;32:817–825. doi:10.1097/cji.0b013e3181ad4d5d

31. Göstring L, Chew MT, Orlova A, Höidén-Guthenberg I, Wennborg A, Carlsson J. Quantification of internalization of EGFR-binding affibody molecules: methodological aspects. *Int J Oncol*. 2010;36:12241–12245. doi:10.3892/ijo_00000551

32. Walsh AS, Yin HF, Erben CM, Wood MJA, Turberfield AJ. DNA cage delivery to mammalian cells. *ACS Nano*. 2011;5:5427–5432. doi:10.1021/nn2005574

33. Li J, Pei H, Zhu B, et al. Self-assembled multivalent DNA nanostructures for noninvasive intracellular delivery of immunostimulatory CpG oligonucleotides. *ACS Nano*. 2011;5:8783–8789. doi:10.1021/nn202774x

34. Gmeiner WH, Debinski W, Milligan C, Caudell D, Pardee TS. The applications of the novel polymeric fluoropyrimidine F10 in cancer treatment: current evidence. *Future Oncol*. 2016;12:2009–2020. doi:10.2217/fon-2016-0091

35. Fojo T, Coley HM. The role of efflux pumps in drug-resistant metastatic breast cancer: new insights and treatment strategies. *Clin Breast Cancer*. 2007;7:749–756. doi:10.3816/CBC.2007.n.035

36. Wu X, He C, Wu Y, Chen X. Synergistic therapeutic effects of Schiff's base cross-linked injectable hydrogels for local co-delivery of metformin and 5-fluorouracil in a mouse colon carcinoma model. *Biomaterials*. 2016;75:148–162. doi:10.1016/j.biomaterials.2015.10.016